LETTER

doi:10.1038/nature12483

Observation of dipolar spin–exchange interactions with lattice-confined polar molecules

Bo Yan[1,2], Steven A. Moses[1,2], Bryce Gadway[1,2], Jacob P. Covey[1,2], Kaden R. A. Hazzard[1,2], Ana Maria Rey[1,2], Deborah S. Jin[1,2] & Jun Ye[1,2]

With the production of polar molecules in the quantum regime[1,2], long-range dipolar interactions are expected to facilitate understanding of strongly interacting many-body quantum systems and to realize lattice spin models[3] for exploring quantum magnetism. In ordinary atomic systems, where contact interactions require wavefunction overlap, effective spin interactions on a lattice can be mediated by tunnelling, through a process referred to as superexchange; however, the coupling is relatively weak and is limited to nearest-neighbour interactions[4,5]. In contrast, dipolar interactions exist even in the absence of tunnelling and extend beyond nearest neighbours. This allows coherent spin dynamics to persist even for gases with relatively high entropy and low lattice filling. Measured effects of dipolar interactions in ultracold molecular gases have been limited to the modification of inelastic collisions and chemical reactions[6,7]. Here we use dipolar interactions of polar molecules pinned in a three-dimensional optical lattice to realize a lattice spin model. Spin is encoded in rotational states of molecules that are prepared and probed by microwaves. Resonant exchange of rotational angular momentum between two molecules realizes a spin-exchange interaction. The dipolar interactions are apparent in the evolution of the spin coherence, which shows oscillations in addition to an overall decay of the coherence. The frequency of these oscillations, the strong dependence of the spin coherence time on the lattice filling factor and the effect of a multipulse sequence designed to reverse dynamics due to two-body exchange interactions all provide evidence of dipolar interactions. Furthermore, we demonstrate the suppression of loss in weak lattices due to a continuous quantum Zeno mechanism[8]. Measurements of these tunnelling-induced losses allow us to determine the lattice filling factor independently. Our work constitutes an initial exploration of the behaviour of many-body spin models with direct, long-range spin interactions and lays the groundwork for future studies of many-body dynamics in spin lattices.

Long-range and spatially anisotropic dipole–dipole interactions permit new approaches for the preparation and exploration of strongly correlated quantum matter that exhibits intriguing phenomena such as quantum magnetism, exotic superfluidity and topological phases[9–13]. Ultracold gases of polar molecules provide highly controllable, long-lived and strongly interacting dipolar systems and have recently attracted intense scientific interest. Samples of fermionic $^{40}K^{87}Rb$ polar molecules, with an electric dipole moment of 0.57 D (ref. 1; 1 D = 3.336×10^{-30} C m), have been prepared near the Fermi temperature, and all degrees of freedom (electronic, vibrational, rotational, hyperfine and external motion) can be controlled at the level of single quantum states[7,14,15].

The surprising discovery of bimolecular chemical reactions of KRb at ultralow temperatures[2,6,7] seemed to be a major challenge in creating novel quantum matter. However, the molecules' motion, and, consequently, their reactions, can be fully suppressed in a three-dimensional (3D) optical lattice, where relatively long lifetimes (>25 s) have been observed[15]. The long-range dipolar interaction can then play the dominant part in the dynamics of the molecular internal degrees of freedom, for example by exchanging two neighbouring molecules' rotational states. With spin encoded in the rotational states of the molecule, these dipolar interactions give rise to spin-exchange interactions, analogous to those that are important in quantum magnetism and high-temperature superconductivity[16]. In a 3D lattice, where each molecule is surrounded by many neighbouring sites, this system represents an intriguing many-body quantum spin system in which excitations can have strong correlations even at substantially less than unit lattice filling[17].

Several features distinguish the interactions in a molecular spin model from those observed in ultracold atomic systems. For the superexchange interaction of atoms in optical lattices[4,5], the short-range nature of the interparticle interactions necessitates a second-order perturbative process to occur in the tunnelling of atoms between lattice sites. Hence, the energy scale of the superexchange interaction decreases exponentially with lattice depth. This spin–motion coupling limits superexchange to nearest-neighbour interactions and requires extremely low temperature and entropy.

In contrast, long-range dipolar interactions decay with separation, r, as $1/r^3$, and interactions beyond nearest neighbours are significant. This long-range interaction allows exploration of coherent spin dynamics in very deep lattices where the molecules' translational motion is frozen and where the absence of tunnelling would preclude the superexchange interactions of atoms. We note that the dipolar interaction is also different from that of electrons, for which an effective spin interaction arises due to the spin-independent Coulomb interaction and the exchange symmetry of the fermionic electrons. In contrast, the dipolar interaction is a direct spin–spin interaction that does not require any wavefunction overlap. In addition to polar molecules, ultracold systems such as magnetic atoms[10,18–20] and trapped ions[21,22] are candidates for realizing coherent, controllable spin models with power-law interactions; however, spin-exchange interactions have yet to be created and observed in these systems. In Rydberg atoms, Förster resonances involving multiple Rydberg states have been observed, albeit with short coherence times[23].

The molecular rotational states $|N, m_N\rangle$, where N is the principal quantum number and m_N is the projection onto the quantization axis, are the focus of our current investigation of a dipolar spin system. In general, an external d.c. electric field induces a dipole moment in the laboratory frame by mixing opposite-parity rotational states. However, even in the absence of a d.c. electric field, dipolar interactions can be established using a microwave field to create a coherent superposition between two rotational states[24], labelled $|\uparrow\rangle$ and $|\downarrow\rangle$. In addition, a microwave field can probe the coherent spin dynamics due to dipolar interactions.

In the absence of an applied electric field, two-level polar molecules trapped in a strong 3D lattice (Fig. 1a) can be described using a spin-1/2 lattice model with the interaction Hamiltonian[12,17,24]

$$H = \frac{J_\perp}{2} \sum_{i>j} V_{\mathrm{dd}}(\boldsymbol{r}_i - \boldsymbol{r}_j)\left(S_i^+ S_j^- + S_i^- S_j^+\right) \qquad (1)$$

[1]JILA, National Institute of Standards and Technology and University of Colorado, Boulder, Colorado 80309, USA. [2]Department of Physics, University of Colorado, Boulder, Colorado 80309, USA.

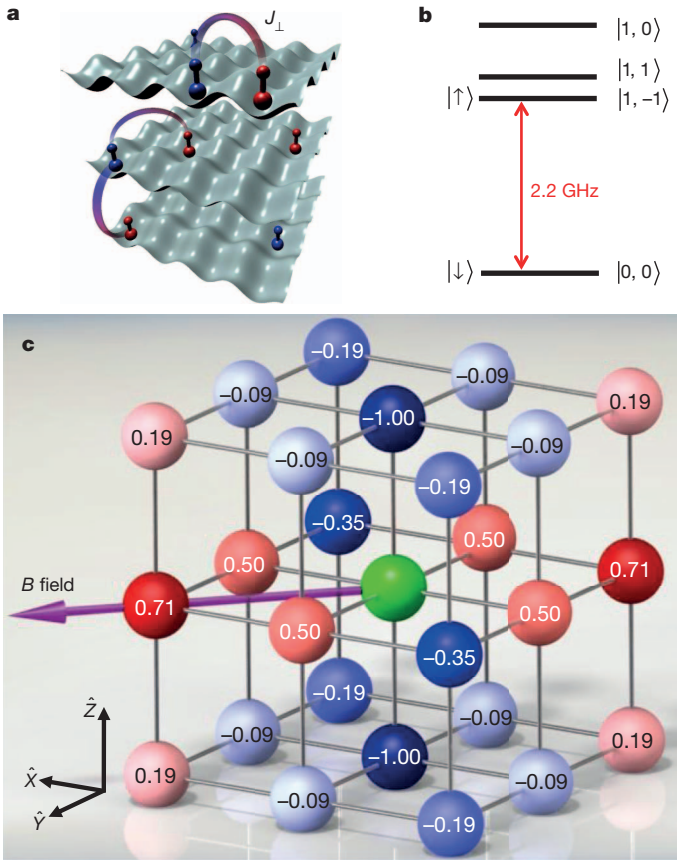

Figure 1 | Dipolar interactions of polar molecules in a 3D lattice. **a**, Polar molecules are loaded into a deep 3D optical lattice. Microwaves are used to address the transition between two rotational states (red and blue represent different rotational states). $J_\perp$ characterizes the spin-exchange interaction energy. **b**, Schematic energy diagram (not to scale) for the ground and first excited rotational states. The degeneracy of the excited rotational states is broken as a result of a weak coupling of the nuclear and rotational degrees of freedom. We use $|0,0\rangle$ and $|1,-1\rangle$ as our two spin states. **c**, The interaction energy between any two molecules depends on their relative position in the lattice. The numbers shown give the geometrical factor $-V_{dd}(\boldsymbol{r}_i-\boldsymbol{r}_j)$ for the dipolar interaction of each site relative to the central site (green), under the specific quantization axis (*B* field). Negative values (blue) correspond to attractive interactions, and positive values (red) correspond to repulsive interactions.

where $S_i^{\pm}$ (along with S_i^z) are the usual spin-1/2 angular momentum operators on site i. The dipolar interaction energy includes a geometrical factor, $V_{dd}(\boldsymbol{r}_i-\boldsymbol{r}_j)=(1-3\cos^2(\Theta_{ij}))/|\boldsymbol{r}_i-\boldsymbol{r}_j|^3$, where the vector $\boldsymbol{r}_i$ is the position of the ith molecule in units of the lattice constant a and Θ_{ij} is the angle between the quantization axis, defined by the B field, and the vector connecting molecules i and j. More generally, polar molecules realize the full spin-1/2 model with the capability of controlling all relevant interaction parameters. In this work, we isolate the spin-exchange interaction, which has been difficult to realize in other systems, by setting the Ising term, which is proportional to $S_i^zS_j^z$, to zero by working at zero electric field. The Hamiltonian reduces to the limiting case known as the spin-1/2 quantum XY model, in which the spin-exchange interaction is characterized by $J_\perp=-d_{\downarrow\uparrow}^2\big/4\pi\varepsilon_0a^3$, where ε_0 is the permittivity of free space and $d_{\downarrow\uparrow}=\langle\downarrow|d|\uparrow\rangle$ is the dipole matrix element between $|\downarrow\rangle$ and $|\uparrow\rangle$. Physically, this term is responsible for exchanging the spins of two trapped molecules (Fig. 1a).

In our experiment, we create up to 2×10^4 ground-state KRb molecules in the lowest motional band of a 3D lattice formed by three mutually orthogonal standing waves with wavelengths of $\lambda=1{,}064$ nm. The lattice constant is $a=\lambda/2$ and the lattice depth is $40E_r$ in each direction, where $E_r=\hbar^2k^2/2m$ is the recoil energy, $\hbar$ is Planck's constant divided by 2π, $k=2\pi/\lambda$ and m is the mass of KRb. We use microwaves at ~2.2 GHz to couple the $|0,0\rangle$ and $|1,-1\rangle$ states, which form the $|\downarrow\rangle$ and $|\uparrow\rangle$ two-level system. The degeneracy of the $N=1$ rotational states is broken by the interaction between the nuclear quadrupole moments and the rotation of the molecules, and in a 54.59 mT magnetic field the $|1,0\rangle$ and $|1,1\rangle$ states are higher in frequency than the $|1,-1\rangle$ state by 270 and 70 kHz, respectively[14] (Fig. 1b). All rotational states used in this work involve the nuclear spin quantum numbers $m_I^{Rb}=1/2$ and $m_I^K=-4$, following the notation of ref. 14. The quantization axis is set by the magnetic field, which is oriented at 45° with respect to the $\hat{X}$ and $\hat{Y}$ lattice directions (Fig. 1c). The polarizations of the lattice beams are chosen such that the tensor a.c. polarizabilities of the $|0,0\rangle$ and $|1,-1\rangle$ states are very similar[25], so that we create a spin-state-independent lattice trap (Methods). We address the entire sample with a microwave field and achieve a π-pulse fidelity of >99%.

The energy scale for our spin-1/2 quantum XY system is characterized by $(J_\perp/2)V_{dd}(\boldsymbol{r}_i-\boldsymbol{r}_j)$. For our rotational states, $|d_{\downarrow\uparrow}|=0.98\times0.57/\sqrt{3}$ D and $|J_\perp/2h|=52$ Hz. Here the additional factor of 0.98 in the transition dipole matrix element comes from an estimated 2% admixture of another hyperfine state[14]. Each molecule in the lattice will experience an interaction energy with contributions from all other molecules, where each contribution depends on molecular separation and angle Θ. Figure 1c shows the geometrical factors for nearby sites relative to a central molecule (green) for our experimental conditions.

We employ coherent microwave spectroscopy to initiate and probe spin dynamics. Figure 2a shows a basic spin-echo pulse sequence and its Bloch sphere representation. Starting with the molecules prepared in $|\downarrow\rangle$, the first $(\pi/2)_y$-pulse creates a superposition state $(|\downarrow\rangle+|\uparrow\rangle)/\sqrt{2}$. Any residual differential a.c. Stark shift, which gives rise to single-particle dephasing, can be removed using a spin-echo pulse. After a free-evolution time of $T/2$, we apply a $(\pi)_y$ echo pulse, which flips the spins and reverses the direction of single-particle precession. The spins rephase after another free-evolution time of $T/2$, at which time we probe the coherence by applying a π/2-pulse with a phase offset relative to the initial pulse. We measure the number of molecules left in $|\downarrow\rangle$ as a function of this offset phase, which yields a Ramsey fringe (Fig. 2b).

With the single-particle dephasing effectively removed, the contrast of the Ramsey fringe as a function of T yields information on spin interactions in the system[26]. We note that the spin-echo pulse has no impact on the dipolar spin-exchange interactions described by equation (1). The most striking feature evident in the measured contrast curves (Fig. 2c, d) is the oscillations on top of an overall decay. We attribute both the contrast decay and the oscillations to dipolar interactions. Imperfect lattice filling and many-body interactions each give a spread of interaction energies, which results in dephasing and a decaying contrast in the Ramsey measurement. Figure 1c illustrates the different interaction energies coming from V_{dd}, which can be positive or negative. For low lattice fillings, the interaction energy spectrum can have a strong contribution from the highest-magnitude nearest-neighbour interaction. Oscillations in the contrast can then result from the beating of this particular frequency with the contribution from molecules that experience negligible interaction shifts. In principle, there should be several different oscillation frequencies owing to the differing geometrical factors in the lattice. Although a dominant oscillation frequency is observed, we note that our data does not rule out additional frequencies.

Because interaction effects depend on the density, we investigate spin coherence for different lattice filling factors. To reduce the density of molecules without changing the distribution, we hold the molecules in the lattice for a few seconds while inducing single-particle losses with an additional strong optical beam that enhances the rate of off-resonance light scattering[15]. We fit the measured time dependence of the Ramsey contrast to an empirical function, $Ae^{-T/\tau}+B\cos^2(\pi fT)$, to extract a coherence time, τ, and an oscillation frequency, f. As shown in Fig. 2d, f is essentially unchanged over our accessible range of densities,

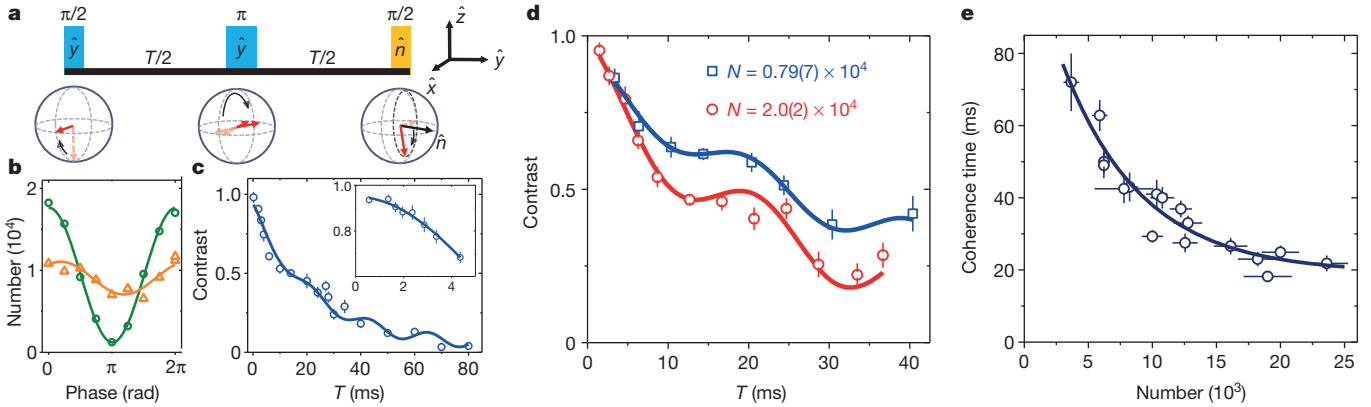

Figure 2 | Coherent spin dynamics of polar molecules. **a**, A $(\pi/2)_y$-pulse initializes the molecules in a coherent superposition of rotational states. A spin-echo pulse sequence is used to correct for effects arising from single-particle inhomogeneities across the sample, such as residual light shifts. **b**, The phase of the final $\pi/2$-pulse is scanned (corresponding to rotations around a variable axis, $\hat{n}$) to obtain a Ramsey fringe. Two fringes are shown, corresponding to the short (green circles) and intermediate timescales (orange triangles). **c**, The contrast of the Ramsey fringe is measured as a function of interrogation time. Because the molecules' spin states are initially all in phase, at very short times, $T < 2h/J_\perp$, the contrast decay curve should be quadratic[17], as shown in the inset. **d**, The contrast of the Ramsey fringe versus interrogation time is shown for two different filling factors, characterized by the initial molecule number. In addition to the density-dependent decay, we observe oscillations, which arise from spin-exchange interactions between neighbouring molecules. **e**, The spin coherence time decreases for increasing molecule number. The solid line shows a fit to $C + A/N$, where C and A are constants. Error bars, 1 s.d.

but τ depends on the number of molecules, or filling fraction. This is a signature of many-body interactions, and the observation agrees with theoretical calculations using a cluster expansion (Methods).

We observe oscillation frequencies in the range 48 ± 2 Hz for molecule numbers in the lattice that vary by threefold. The fact that this frequency is consistent with the largest nearest-neighbour interaction energy, $|J_\perp/2h| = 52$ Hz, supports the conclusion that the contrast oscillations come from nearest-neighbour dipole–dipole interactions. Because this frequency is determined by the lattice geometry and the dipole matrix element, it does not depend on the lattice filling factor. We also confirm that the oscillation frequency does not depend on the lattice depth from $20E_r$ to $50E_r$ (Methods). For the coherence time, we observe a strong dependence on the filling factor (Fig. 2e). Density dependence is a classic signature of interaction effects, and we conclude that the coherence time in the deep lattice is limited by dipole–dipole interactions. For higher filling factors, the increasing probability that molecules have multiple neighbours means that more spin-exchange frequencies will contribute to the signal, which leads to faster dephasing.

Multipulse sequences, as well as single spin-echo pulses, are examples of dynamical decoupling, which is widely used in NMR[27] and quantum information processing[28] to remove dephasing and extend coherence times. Although a spin-echo pulse cannot mitigate the contrast decay that arises from dipole–dipole interactions, a multipulse sequence can. In particular, the pulse sequence[27] shown in Fig. 3a is designed to remove dephasing due to two-particle dipolar interactions (Methods). Analogous to how a spin-echo pulse works, this pulse sequence swaps the eigenstates of the dipolar interaction Hamiltonian (equation (1)) for two isolated particles to allow for subsequent rephasing.

Figure 3b summarizes the decay of the Ramsey contrast for three different pulse sequences. With a simple two-pulse Ramsey sequence (with no spin-echo pulse), the coherence time of the system is very short, with the fringe contrast decaying within 1 ms (Fig. 3b, triangles). With the addition of a single spin-echo pulse, the single-particle dephasing time can be extended to ~80 ms (measured for our lowest molecular density). However, this coherence time is reduced drastically with increasing molecule number in the lattice, and we observe oscillations in the contrast signal (Fig. 3b, circles). When we apply the multipulse sequence, the oscillations in the contrast are suppressed and the data fit well a simple exponential decay with a coherence time slightly longer than that of the spin-echo case (Fig. 3b, squares). The

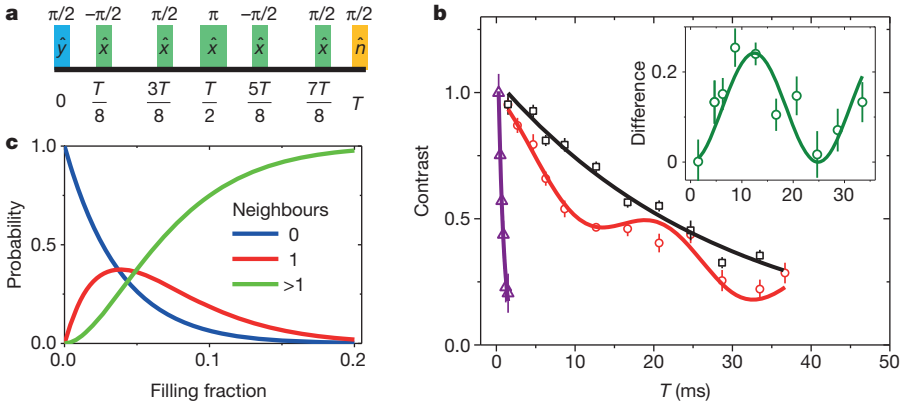

Figure 3 | Multipulse sequence and decoupling of pairwise dipolar interactions. **a**, The multipulse sequence is designed to suppress both single-particle dephasing and the effect of pairwise dipole–dipole interactions. **b**, The contrast decay is displayed as a function of time for three different pulse sequences. Without a spin-echo pulse, single-particle inhomogeneities result in a Ramsey coherence time of ~1 ms (triangles). The spin-echo pulse effectively removes the single-particle dephasing, such that spin-exchange interactions play the dominant role in the contrast decay (circles). The multipulse sequence suppresses the contrast oscillations and slightly improves the coherence time (squares). Inset, the difference in contrast between the multipulse sequence and the spin-echo case shows oscillations. Error bars, 1 s.d. **c**, The probability of a particular molecule having zero, one or more than one neighbours (within the cube shown in Fig. 1c) is plotted as a function of a uniform lattice filling factor.

differences in the measured contrast oscillations and decay for the usual spin-echo and multipulse sequence highlight the spin-exchange dynamics driven by pairwise dipolar interactions (Fig. 3b, inset).

To understand the dynamics of this spin system, a key ingredient is the filling fraction of molecules in the 3D lattice, because the Ramsey contrast decay depends sensitively on the molecular density (Fig. 2e). Figure 3c shows the probabilities of a particular molecule having zero, one or more than one neighbours. The probability of having two or more neighbours is non-negligible even for relatively low fillings. The contrast oscillation is dominated by contributions from pairs of molecules, whereas interactions of multiple molecules contribute mainly to the contrast decay.

To provide an independent determination of the filling fraction, we have measured tunnelling-induced loss at reduced lattice depths. Molecules are initially prepared in $|\downarrow\rangle$ in a $40E_r$ lattice. For our fermionic molecules, the chemical reaction rate is much larger between molecules in distinguishable internal states[2]. Moreover, Pauli blocking strongly suppresses the tunnelling of molecules in the same spin state into the same lattice site. Therefore, we create a 50:50 incoherent spin mixture of $|\downarrow\rangle$ and $|\uparrow\rangle$ by applying a $\pi/2$-pulse and waiting 50 ms. We then quickly (within 1 ms) lower the lattice depth along only a single direction ($\hat{Y}$, as shown in Fig. 4a) to allow tunnelling and loss due to on-site chemical reactions[2,6,7]. We then measure the remaining number of molecules in the $|\downarrow\rangle$ state as a function of the holding time. Figure 4b shows example loss curves for two different lattice depths along $\hat{Y}$.

In our system, the on-site loss rate, Γ_0, is proportional to the chemical reaction rate between the $|0,0\rangle$ and $|1,-1\rangle$ molecules[7]:

$$\Gamma_0 = \beta \int |W(X,Y,Z)|^4 \mathrm{d}X\ \mathrm{d}Y\ \mathrm{d}Z \qquad (2)$$

Here $\beta = 9.0(4) \times 10^{-10}\ \mathrm{cm^3\ s^{-1}}$ (parenthetical error, s.d.) is the two-body loss coefficient (Methods) and $W(X, Y, Z)$ is the ground-band Wannier function. We can modify Γ_0 by changing the lattice depth; however, for our measurements, the system always remains in the strongly interacting regime, in which $\Gamma_0 \gg J_t/\hbar$, where J_t is the tunnelling amplitude. This is the regime of the continuous quantum Zeno effect[8,29], where dissipation in the form of measurement or loss can lead to suppression of coherent processes such as tunnelling. Thus, increasing Γ_0 actually decreases the effective two-body loss rate between neighbouring molecules, which is given by

$$\Gamma_{\mathrm{eff}} = \frac{2(J_t/\hbar)^2}{\Gamma_0} \qquad (3)$$

The number of $|\downarrow\rangle$ molecules, $N_\downarrow(t)$, can then be described with a two-body loss equation

$$\frac{\mathrm{d}N_\downarrow(t)}{\mathrm{d}t} = -\frac{\kappa}{N_{\downarrow,0}} N_\downarrow(t)^2 \qquad (4)$$

where $N_{\downarrow,0}$ is the initial number of $|\downarrow\rangle$ molecules and the loss rate coefficient is given by[30] $\kappa = 4q\Gamma_{\mathrm{eff}} g^{(2)}_{\downarrow\uparrow} n_{\downarrow,0}$. Here $2n_{\downarrow,0} = n_0$ is the initial filling fraction in the lattice, $q = 2$ is the number of nearest-neighbour sites in our one-dimensional tunnelling geometry and $g^{(2)}_{\downarrow\uparrow}$ is the correlation function of different spin states for nearest-neighbouring sites i and j: $g^{(2)}_{\downarrow\uparrow} = \langle \hat{n}_i \hat{n}_j - 4\vec{S}_i \cdot \vec{S}_j \rangle / \langle \hat{n}_i \rangle^2$, with $\hat{n}_i$ the number operator at site i and $\vec{S}_i$ the spin-1/2 vector operator. In our case, we assume that the molecules are initially randomly distributed in the $|\downarrow\rangle$ and $|\uparrow\rangle$ states, so that $g^{(2)}_{\downarrow\uparrow} = 1$. Because the redistribution of molecules due to losses and tunnelling can modify $g^{(2)}_{\downarrow\uparrow}$, we fit the data to the solution of equation (4) for short times, where the number has changed by less than 50%.

We verify the scaling of the continuous quantum Zeno effect by measuring the dependence of the loss rate, κ, on Γ_0 and J_t. To study the dependence on Γ_0, we set the lattice depth along $\hat{Y}$ to be $5.4(4)E_r$, which fixes J_t, and then increase the lattice depths along the $\hat{X}$ and $\hat{Z}$

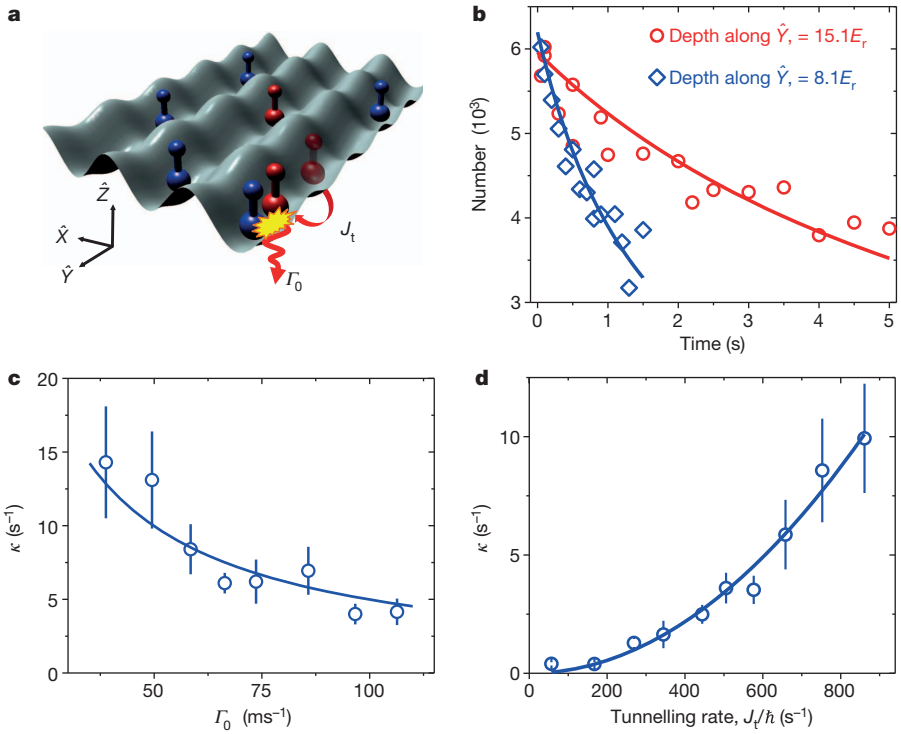

Figure 4 | Quantum Zeno effect for polar molecules in a 3D lattice. **a**, The lattice depths along $\hat{X}$ and $\hat{Z}$ are kept at $40E_r$, whereas the lattice depth along $\hat{Y}$ is reduced to allow tunnelling along the $\hat{Y}$ direction at a rate $J_t/\hbar$. Once two molecules in different spin states tunnel to the same site, they are lost owing to chemical reactions occurring at rate Γ_0. **b**, Number of $|\downarrow\rangle$ molecules versus time is shown for lattice depths along $\hat{Y}$ of $8.1E_r$ and $15.1E_r$. **c**, The number loss rate, κ, has a $1/\Gamma_0$ dependence (fit shown), which is consistent with the quantum Zeno effect. **d**, The number loss rate, κ, has a J_t^2 dependence (fit shown), as predicted from the quantum Zeno effect. Error bars, 1 s.d.

directions. This compresses the wave function $W(X, Y, Z)$ at each lattice site, and thus increases Γ_0. As expected for the quantum Zeno regime, the measured κ decreases as Γ_0 increases, and the data are consistent with $\kappa \propto 1/\Gamma_0$ (Fig. 4c). To study the dependence on J_t, we vary the lattice depth along $\hat{Y}$, while adjusting the $\hat{X}$ and $\hat{Z}$ lattice depths to keep Γ_0 fixed. As shown in Fig. 4d, the measured κ exhibits a quadratic dependence on J_t as predicted by equation (3). For these loss rate measurements, all parameters are known except the initial filling fraction, n_0. From measurements of the loss rate at several lattice depths, our simple model gives $n_0 = 25(5)\%$ for 2×10^4 molecules. However, a more complete theory that incorporates interaction-modified Wannier functions in the lattice will lower this value. We note that calculations of the Ramsey fringe contrast decay using a cluster expansion give an estimated n_0 of $\sim$10% (Methods), which is more consistent with an estimation of the filling based on direct imaging.

Although it is desirable to increase the lattice filling to explore interesting phases such as quantum magnetism or exotic superfluidity, we have seen that the modest filling factors achieved in our experiment already enable the observation of dipolar interaction effects in a 3D lattice spin model. Furthermore, this work prepares us for the study of non-trivial dynamic processes such as many-body localization of spin excitations. Adding an external electric field would further increase the variety of spin models that can be realized with this system.

METHODS SUMMARY

We begin with $\sim 1 \times 10^5$ ^{87}Rb atoms and 2.5×10^5 ^{40}K atoms in a far off-resonance dipole trap at 1,064 nm. The trap frequencies are 25 Hz radially and 185 Hz axially for Rb, where the axial direction is along $\hat{Z}$. The Rb gas is a Bose–Einstein condensate with $T/T_c \approx 0.5$ and the K Fermi gas is at $T/T_F \approx 0.5$, where T_c is the transition temperature for the condensate and T_F is the Fermi temperature. We smoothly ramp on a 3D lattice over 100 ms to a final depth of $40E_r$ (16 and 7 recoil energies for Rb and K atoms, respectively). The $\hat{X}$ and $\hat{Y}$ lattice beams have waists of 200 μm and the $\hat{Z}$ beam has a waist of 250 μm. The lattice depth is calibrated with parametric heating of the molecular gas[25] and has an estimated uncertainty of 5%. After turning on the lattice, we lower the intensity of the dipole trap to zero in 50 ms, and then ramp a magnetic field from 54.89 to 54.59 mT in 1 ms to create weakly bound KRb Feshbach molecules. We then use two-photon stimulated Raman adiabatic passage to transfer the Feshbach molecules to the rovibrational ground state. The unpaired Rb and K atoms are removed using resonant light scattering. From band-mapping measurements, we find that the fraction of molecules in higher bands is consistent with zero within our detection limit of 5%. To measure the number of ground-state molecules in the lattice, we reverse the two-photon stimulated Raman adiabatic passage to recreate Feshbach molecules, and then take an absorption image using light resonant with the K cycling transition.

Full Methods and any associated references are available in the online version of the paper.

Received 17 May; accepted 16 July 2013.
Published online 18 September 2013.

1. Ni, K.-K. *et al.* A high phase-space-density gas of polar molecules. *Science* **322,** 231–235 (2008).
2. Ospelkaus, S. *et al.* Quantum-state controlled chemical reactions of ultracold potassium-rubidium molecules. *Science* **327,** 853–857 (2010).
3. Micheli, A., Brennen, G. K. & Zoller, P. A toolbox for lattice-spin models with polar molecules. *Nature Phys.* **2,** 341–347 (2006).
4. Trotzky, S. *et al.* Time-resolved observation and control of superexchange interactions with ultracold atoms in optical lattices. *Science* **319,** 295–299 (2008).
5. Greif, D., Uehlinger, T., Jotzu, G., Tarruell, L. & Esslinger, T. Short-range quantum magnetism of ultracold fermions in an optical lattice. *Science* **340,** 1307–1310 (2013).
6. Ni, K.-K. *et al.* Dipolar collisions of polar molecules in the quantum regime. *Nature* **464,** 1324–1328 (2010).
7. de Miranda, M. H. G. *et al.* Controlling the quantum stereodynamics of ultracold bimolecular reactions. *Nature Phys.* **7,** 502–507 (2011).
8. Syassen, N. *et al.* Strong dissipation inhibits losses and induces correlations in cold molecular gases. *Science* **320,** 1329–1331 (2008).
9. Carr, L. D., DeMille, D., Krems, R. V. & Ye, J. Cold and ultracold molecules: science, technology and applications. *New J. Phys.* **11,** 055049 (2009).
10. Lahaye, T., Menotti, C., Santos, L., Lewenstein, M. & Pfau, T. The physics of dipolar bosonic quantum gases. *Rep. Prog. Phys.* **72,** 126401 (2009).
11. Potter, A. C., Berg, E., Wang, D.-W., Halperin, B. I. & Demler, E. Superfluidity and dimerization in a multilayered system of fermionic polar molecules. *Phys. Rev. Lett.* **105,** 220406 (2010).
12. Gorshkov, A. V. *et al.* Tunable superfluidity and quantum magnetism with ultracold polar molecules. *Phys. Rev. Lett.* **107,** 115301 (2011).
13. Yao, N. Y. *et al.* Topological flat bands from dipolar spin systems. *Phys. Rev. Lett.* **109,** 266804 (2012).
14. Ospelkaus, S. *et al.* Controlling the hyperfine state of rovibronic ground-state polar molecules. *Phys. Rev. Lett.* **104,** 030402 (2010).
15. Chotia, A. *et al.* Long-lived dipolar molecules and Feshbach molecules in a 3D optical lattice. *Phys. Rev. Lett.* **108,** 080405 (2012).
16. Lee, P. A., Nagaosa, N. & Wen, X.-G. Doping a Mott insulator: physics of high-temperature superconductivity. *Rev. Mod. Phys.* **78,** 17–85 (2006).
17. Hazzard, K. R. A., Manmana, S. R., Foss-Feig, M. & Rey, A. M. Far-from-equilibrium quantum magnetism with ultracold polar molecules. *Phys. Rev. Lett.* **110,** 075301 (2013).
18. Lu, M., Burdick, N. Q. & Lev, B. L. Quantum degenerate dipolar Fermi gas. *Phys. Rev. Lett.* **108,** 215301 (2012).
19. Aikawa, K. *et al.* Bose–Einstein condensation of erbium. *Phys. Rev. Lett.* **108,** 210401 (2012).
20. de Paz, A. *et al.* Resonant demagnetization of a dipolar BEC in a 3D optical lattice. *Phys. Rev. A* **87,** 051609(R) (2013).
21. Britton, J. W. *et al.* Engineered two-dimensional Ising interactions in a trapped-ion quantum simulator with hundreds of spins. *Nature* **484,** 489–492 (2012).
22. Islam, R. *et al.* Emergence and frustration of magnetism with variable-range interactions in a quantum simulator. *Science* **340,** 583–587 (2013).
23. Nipper, J. *et al.* Atomic pair-state interferometer: controlling and measuring an interaction-induced phase shift in Rydberg-atom pairs. *Phys. Rev. X* **2,** 031011 (2012).
24. Barnett, R., Petrov, D., Lukin, M. & Demler, E. Quantum magnetism with multicomponent dipolar molecules in an optical lattice. *Phys. Rev. Lett.* **96,** 190401 (2006).
25. Neyenhuis, B. *et al.* Anisotropic polarizability of ultracold polar KRb molecules. *Phys. Rev. Lett.* **109,** 230403 (2012).
26. Martin, M. J. *et al.* A quantum many-body spin system in an optical lattice clock. *Science* **341,** 632–636 (2013).
27. Waugh, J. S., Huber, L. M. & Haeberlen, U. Approach to high-resolution NMR in solids. *Phys. Rev. Lett.* **20,** 180–182 (1968).
28. Maurer, P. C. *et al.* Room-temperature quantum bit memory exceeding one second. *Science* **336,** 1283–1286 (2012).
29. Itano, W. M., Heinzen, D. J., Bollinger, J. J. & Wineland, D. J. Quantum Zeno effect. *Phys. Rev. A* **41,** 2295–2300 (1990).
30. Baur, S. K. & Mueller, E. J. Two-body recombination in a quantum-mechanical lattice gas: entropy generation and probing of short-range magnetic correlations. *Phys. Rev. A* **82,** 023626 (2010).

Supplementary Information is available in the online version of the paper.

Acknowledgements We thank B. Zhu, M. Foss-Feig, G. Quéméner and M. Lukin for discussions. We acknowledge funding for this work from the NIST, NSF, AFOSR-ARO (MURI), ARO, DOE and ARO-DARPA-OLE. S.A.M. is supported by an NDSEG Graduate Fellowship. B.G. and K.R.A.H. are National Research Council postdoctoral fellows. K.R.A.H. and A.M.R. thank the KITP for hospitality.

Author Contributions The experimental work and data analysis were carried out by B.Y., S.A.M., B.G., J.P.C., D.S.J. and J.Y. Theoretical modelling and calculations were done by K.R.A.H. and A.M.R. All authors discussed the results and contributed to the preparation of the manuscript.

Author Information Reprints and permissions information is available at www.nature.com/reprints. The authors declare no competing financial interests. Readers are welcome to comment on the online version of the paper. Correspondence and requests for materials should be addressed to D.S.J. (jin@jilau1.colorado.edu) or J.Y. (ye@jila.colorado.edu).

METHODS

Preparation of molecules in a 3D optical lattice. We begin with $\sim 1 \times 10^5$ ^{87}Rb atoms and 2.5×10^5 ^{40}K atoms in a far off-resonance dipole trap at 1,064 nm. The trapping frequencies are 25 Hz radially and 185 Hz axially for Rb, where the axial direction is along $\hat{Z}$. The Rb gas is a Bose–Einstein condensate with $T/T_c \approx 0.5$, and the K Fermi gas is at $T/T_F \approx 0.5$, where T_c is the transition temperature for the condensate and T_F is the Fermi temperature. We smoothly ramp on a 3D lattice over 100 ms to a final depth of $40E_r$ (16 and 7 recoil energies for Rb and K atoms, respectively). The $\hat{X}$ and $\hat{Y}$ lattice beams have waists of 200 μm and the $\hat{Z}$ beam has a waist of 250 μm. We calibrate the lattice depth through parametric heating of the molecular gas[25], which results in an estimated uncertainty of 5%. After turning on the lattice, we lower the intensity of the dipole trap to zero in 50 ms, and then ramp a magnetic field from 54.89 to 54.59 mT in 1 ms to create weakly bound KRb Feshbach molecules. We then use two-photon stimulated Raman adiabatic passage to transfer the Feshbach molecules to the rovibrational ground state. The unpaired Rb and K atoms are removed using resonant light scattering. After molecules are created in the lattice, we can perform band-mapping measurements by turning off the lattice in 1 ms. We find that the fraction of molecules in higher bands is consistent with zero within our detection limit of 5%. To measure the number of ground-state molecules in the lattice, we reverse the two-photon stimulated Raman adiabatic passage to recreate Feshbach molecules, and then take an absorption image using light resonant with the K cycling transition.

Differential light shift in a 3D optical lattice. Molecules have complex internal structure; hence, there are a number of different approaches to finding a 'magic' trap that matches the polarizabilities of two different internal states. Because the polarizability of molecules is anisotropic, tuning the angle between the quantization axis and the polarization of the light field can change the polarizabilities[25]. For a 3D lattice, there are three different polarization vectors. The lattice geometry in our experiment is shown in Fig. 1c. We choose the $\hat{X}$ and $\hat{Y}$ lattice beams to have their polarizations along the horizontal plane, at angles of $\pm 45^\circ$ relative to the magnetic field. The $\hat{Z}$ lattice polarization is the same as that of the $\hat{X}$ lattice. Following our previous work[25], the energy shifts for the $|1,0\rangle$, $|1,-1\rangle$ and $|1,1\rangle$ states are determined by finding the eigenvalues of the Hamiltonian

$$H = -\alpha(45^\circ)I_X - \alpha(-45^\circ)I_Y - \alpha(45^\circ)I_Z + \mathrm{diag}(\varepsilon_1,\varepsilon_2,\varepsilon_3) \qquad (5)$$

where I_X, I_Y and I_Z are respectively the intensities of lattice beams along the $\hat{X}$, $\hat{Y}$ and $\hat{Z}$ directions, α is the polarizability matrix defined in ref. 25, and ε_1, ε_2 and ε_3 are respectively the bare energies for $|0,0\rangle$, $|1,-1\rangle$ and $|1,1\rangle$.

Supplementary Fig. 1 shows the differential light shift (with respect to $|0,0\rangle$) of $|1,0\rangle$, $|1,-1\rangle$ and $|1,1\rangle$ as a function of the lattice depth. The state $|1,-1\rangle$ has the smallest intensity dependence, which corresponds to minimal inhomogeneity due to spatial variations of the light shift. The inset shows an expanded plot for $|1,-1\rangle$. The red points are the experimentally measured transition frequencies for different lattice depths, which agree well with theory. When the lattice depth is $\sim 40E_r$ in each direction, the differential light shift is zero. We measure the transition frequency between $|0,0\rangle$ and $|1,-1\rangle$ in a $40E_r$ lattice to be 2.22778338(8) GHz, which agrees with the measured frequency, 2.22778335(4) GHz, in the absence of any optical potentials. At this lattice depth, the slope for the differential light shift is 120 Hz/E_r. The total variation of the light shift across the sample is less than 500 Hz, as estimated from the Ramsey decay time in absence of spin echo.

This residual light shift limits the coherence time of our standard Ramsey measurement to $\sim$1 ms (triangle data points in Fig. 3c), and so we use a spin-echo pulse to mitigate the effects of single-particle dephasing. However, spatial variations of the differential light shift can in principle still influence the spin dynamics. Site-dependent shifts of the resonance frequency would appear in the Hamiltonian as an inhomogeneous 'magnetic field' term, $\delta_i S_i^z$, which can suppress spin exchange. For the conditions used in our experiments, we estimate that the spatial variations of the differential light shift are small enough that spin exchange remains near-resonant. On the basis of the measured Ramsey coherence times and the details of our system (optical lattice beams and the molecular ensemble), we calculate a system-averaged nearest-neighbour bias ($\langle|\delta_i - \delta_{i+1}|\rangle/h$) of 6 Hz, which is well below the expected exchange coupling, $|J_\perp/2h| = 52$ Hz. For neighbours separated by $\sqrt{2}a$ and $2a$, the corresponding shifts are 9 and 13 Hz, respectively. To demonstrate that the oscillation frequency in the Ramsey fringe contrast does not sensitively depend on the optical intensity, we made Ramsey contrast measurements (Supplementary Fig. 2) for values of the lattice depth between $20E_r$ and $40E_r$ and found very good agreement among them.

Multipulse sequence. It is straightforward to understand how the multipulse sequence works for the case of two particles. With two molecules initially prepared in $|\downarrow\downarrow\rangle$, an initial $(\pi/2)_y$-pulse transfers them to

$$\frac{1}{\sqrt{2}}(|\downarrow\rangle + |\uparrow\rangle) \otimes \frac{1}{\sqrt{2}}(|\downarrow\rangle + |\uparrow\rangle) = \frac{1}{2}(|\downarrow\downarrow\rangle + |\uparrow\uparrow\rangle + |\downarrow\uparrow\rangle + |\uparrow\downarrow\rangle) \qquad (6)$$

Because of the spin-exchange term, $|\downarrow\uparrow\rangle$ and $|\uparrow\downarrow\rangle$ are not eigenstates of the Hamiltonian in equation (1). However, the three triplet states $|\downarrow\downarrow\rangle$, $|\uparrow\uparrow\rangle$ and $(|\downarrow\uparrow\rangle + |\uparrow\downarrow\rangle)/\sqrt{2}$ are eigenstates of the Hamiltonian, with eigenenergies 0, 0 and $J_\perp/2$, respectively. We note that a single $(\pi/2)_x$-pulse can swap the states $|\downarrow\downarrow\rangle + |\uparrow\uparrow\rangle$ and $|\downarrow\uparrow\rangle + |\uparrow\downarrow\rangle$, and can thus act as an effective spin echo for these contributions to the two-particle wavefunction.

During the first free-evolution time, of duration $T/8$, $|\downarrow\downarrow\rangle$ and $|\uparrow\uparrow\rangle$ accumulate no phase, whereas $(|\downarrow\uparrow\rangle + |\uparrow\downarrow\rangle)/\sqrt{2}$ accumulates a phase $e^{-i(J_\perp/\hbar)T/16}$. At this point the state is entangled. We then apply a $(-\pi/2)_x$-pulse to swap the contributions from $|\downarrow\uparrow\rangle + |\uparrow\downarrow\rangle$ and $|\downarrow\downarrow\rangle + |\uparrow\uparrow\rangle$. This can alternatively be viewed as swapping the accrued phases. After another free-evolution time, of $T/4$, the $(\pi/2)_x$-pulse swaps the phases again. This state then freely evolves for another time $T/8$, after which both $|\downarrow\uparrow\rangle + |\uparrow\downarrow\rangle$ and $|\downarrow\downarrow\rangle + |\uparrow\uparrow\rangle$ have accumulated the same phase, $e^{-i(J_\perp/\hbar)T/8}$, and the state is, as a result, no longer entangled. In this way, the dephasing due to pairwise dipole–dipole interactions is cancelled. The centre $(\pi)_x$-pulse and another pair of $(-\pi/2)_x$- and $(\pi/2)_x$-pulses are necessary for removing the single-particle inhomogeneity in addition to rephasing the dipole–dipole interactions. The effects of dipole–dipole interactions beyond that of isolated pairs of molecules are not removed by this particular multipulse sequence.

Interspecies two-body loss coefficient. To determine the appropriate two-body loss coefficient to describe the recombination of molecules in distinguishable rotational states, we measured losses for an incoherent mixture of $|0,0\rangle$ and $|1,-1\rangle$ molecules in an optical dipole trap, as presented in Supplementary Fig. 3. We find a two-body loss coefficient of $9.0(4) \times 10^{-10}$ cm^3 s^{-1} for the mixture of rotational states that support resonant dipolar interactions[31]. This exceeds the value for molecules in different nuclear (hyperfine) states[2] (with no resonant dipolar coupling) by a factor of $\sim$5.

Theoretical modelling of the spin dynamics. Theoretical modelling of the spin dynamics observed with Ramsey spectroscopy shows similar oscillations and coherence times as our measurements, and the comparison can be used to estimate a filling factor of 5–10% for 10^4 molecules. Although exactly treating the many-body dynamics is intractable, at sufficiently small filling a 'cluster expansion' can be quite accurate. Here we separate N molecules into clusters, each containing at most 10 molecules, and solve exactly the spin dynamics within these clusters, neglecting intercluster interactions[32,33].

Results on the oscillation frequency, amplitude and decay time for the Ramsey contrast produced by the cluster expansion are all consistent with the experimental observations. We find that the cluster expansion depends relatively weakly on the assumed spatial distribution of the molecules (which we know only roughly), and that the main dependence of the contrast decay comes from the assumed filling, such that the filling estimate stated in the main text is reliable in this regard. A discussion of the convergence of the cluster expansion is far beyond the scope of the present work, but its uncertainties are the main source of the uncertainty in the estimated filling fraction.

The cluster expansion also indicates that the Ramsey contrast decay arises from many-body interaction effects other than either nearest-neighbour interactions or summing the dynamics of pairs of molecules. Although summing pairwise dynamics leads to a contrast decay time, τ, that decreases with increasing filling fraction, this τ is significantly larger than the cluster expansion results and requires unreasonably high lattice filling to match experimental results.

31. Quéméner, G., Bohn, J. L., Petrov, A. & Kotochigova, S. Universalities in ultracold reactions of alkali-metal polar molecules. *Phys. Rev. A* **84,** 062703 (2011).
32. Witzel, W. M., de Sousa, R. & Das Sarma, S. Quantum theory of spectral-diffusion-induced electron spin decoherence. *Phys. Rev. B* **72,** 161306 (2005).
33. Maze, J. R., Taylor, J. M. & Lukin, M. D. Electron spin decoherence of single nitrogen-vacancy defects in diamond. *Phys. Rev. B* **78,** 094303 (2008).